Bulletin of Mathematical Biology (2007) 69: 2405–2428
DOI 10.1007/s11538-007-9225-x

ORIGINAL ARTICLE

Cell Proliferation and Oxygen Diffusion in a Vascularising Scaffold

Kerry A. Landman*, Anna Q. Cai

Department of Mathematics and Statistics, University of Melbourne, Victoria 3010, Australia

Received: 26 October 2006 / Accepted: 25 April 2007 / Published online: 7 June 2007

Abstract The supply of oxygen to proliferating cells within a scaffold is a key factor for the successful building of new tissue in soft tissue engineering applications. A recent in vivo model, where an arteriovenous loop is placed in a scaffold, allows a vascularising network to form within a scaffold, establishing an oxygen source within, rather than external, to the scaffold. A one-dimensional model of oxygen concentration, cell proliferation and cell migration inside such a vascularising scaffold is developed and investigated. In addition, a vascularisation model is presented, which supports a vascularisation front which moves at a constant speed. The effects of vascular growth, homogenous and heterogenous seeding, diffusion of cells and critical hypoxic oxygen concentration are considered. For homogenous seeding, a relationship between the speed of the vascular front and a parameter defining the rate of oxygen diffusion relative to the rate of oxygen consumption determines whether a hypoxic region exists at some time. In particular, an estimate of the length of time that a fixed point in the scaffold will remain under hypoxic conditions is determined. For heterogenous seeding, a Fisher-like travelling wave of cells is established behind the vascular front. These findings provide a fundamental understanding of the important interplay between the parameters and allows for a theoretical assessment of a seeding strategy in a vascularising scaffold.

Keywords Cell migration · Proliferation · Oxygen transport · Vascular · Scaffold · Tissue engineering

1. Introduction

Tissue engineering has the potential to build new tissue to replace failed or damaged organs or tissues (Langer and Vacanti, 1993). An important advance towards synthesising engineered tissue has been the development of porous biodegradable polymer scaffolds which provide a structure on which cells adhere, proliferate and migrate (Agrawal and Ray, 2001).

*Corresponding author.
E-mail address: k.landman@ms.unimelb.edu.au (Kerry A. Landman).

Oxygen and nutrient transport to cells is vital for the success of tissue engineering (Kellner et al., 2002). If oxygen concentrations are inadequate, cell proliferation ceases and cell viability begins to break down. Indeed, under hypoxic conditions (that is in low oxygen concentration conditions), cells convert glucose to lactic acid (Boutilier and St-Pierre, 2000) and necrosis begins to occur. Tolerance to hypoxic conditions differs widely between cell types. Some cells can survive for several hours under mild hypoxic conditions, but only for several minutes under zero oxygen conditions (Boutilier and St-Pierre, 2000). Success in growing new tissue on scaffolds has been limited to sizes of only a few hundred micrometres, because of the inadequacy of the oxygen supply.

For soft tissue engineering applications, such as adipose tissue for breast reconstructive surgery (Patrick, 2000, 2001) or muscle (Agrawal and Ray, 2001) and liver (Hasirci et al., 2001) tissue, large volumes of cells must be built on large scaffolds (for example, up to 60 mm in diameter). If the oxygen supply is limited to the exterior of a scaffold of this magnitude, it is well known that the oxygen levels within a tissue construct quickly reach hypoxic levels. When cells are seeded uniformly throughout the scaffold, then the cells near the oxygen source consume oxygen and proliferate; consequently the cells distant from the source are quickly subjected to hypoxic conditions. The cell population density quickly becomes non-uniform and varies throughout the scaffold; large hypoxic regions persist over long times (Malda et al., 2004).

In principle, these limitations may be avoided by establishing an oxygen supply interior to the scaffold. An in vivo model has recently been developed for this purpose (Cassell et al., 2001). An arteriovenous (A-V) loop from a rat or mouse is placed on a scaffold base and then a dome-shaped scaffold placed on top. The whole device is enclosed in a polycarbonate chamber and placed in the groin of a rat or mouse. Over time, a vascularised network of capillaries forms from the A-V loop to fill the chamber, thus bringing a blood supply to the interior of the scaffold.

The aim of such an in vivo model is to eliminate the development of hypoxic conditions, or at least ensure that the length of time that cells remain under hypoxic conditions is short enough so that there is no permanent damage. The efficacy of such models has not been assessed because of the difficulties in measuring oxygen concentrations over time at different points inside the scaffold.

A mathematical model of oxygen concentrations and cell proliferation inside a scaffold is an important tool in assessing and planning tissue engineering outcomes. Several groups have considered oxygen diffusion and cell proliferation inside a scaffold, where the oxygen source is external to the scaffold. Various oxygen consumption and diffusion rates have been considered and their effect on cell count with time have been analysed (Galban and Locke, 1997, 1999a; 1999b). Lewis et al. (2005) developed a model of the spatial and temporal distribution of oxygen and cell density and compared the results with experimental data of Malda et al. (2004). Their conclusions give a proliferation-dominated region at the scaffold edge closest to the oxygen source, which decreases in thickness as time progresses. By assuming that oxygen consumption was a constant (independent of oxygen concentration), some revealing mathematical analysis determined the evolution of a hypoxic, non-proliferating cell region. The boundary separating this hypoxic region from the proliferating region ($t = \tau(x)$) progressed from the far end of the scaffold into the scaffold interior towards the oxygen source, moving at an exponentially decaying rate, as illustrated in Fig. 1. Therefore, any fixed point x inside the scaffold will remain under hypoxic conditions for all time $t > \tau(x)$.

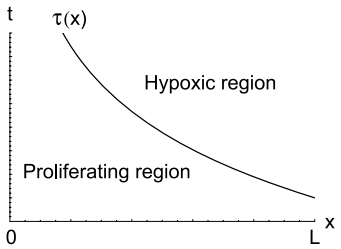

Fig. 1 Schematic space-time diagram indicating the proliferating and hypoxic regions for a scaffold $0 < x < L$, with a fixed oxygen source at $x = 0$ from the analysis by Lewis et al. (2005). The curve $\tau(x)$ is the boundary between these two regions; it moves at an exponentially decaying rate towards $x = 0$.

Croll et al. (2005) developed a model of the oxygen diffusion and cell density in the in vivo A-V loop chamber. A hemi-spherical annular region was considered. The inner radius was the capillary front and the capillaries were assumed to grow outwards in the radial direction with a constant speed. The cells' oxygen consumption was described by Michaelis–Menten kinetics. Oxygen and cell density as a function of position in the scaffold and time were determined numerically for different speeds of the capillary front and various model parameter values. Both homogenous and heterogenous seeding strategies were assessed. Croll et al. concluded that a homogenous cell density seeding strategy, even with a moving oxygen source provided via vascularisation, gives rise to hypoxic conditions in some regions of the scaffold for an unacceptable period of time. The most promising strategy was found to be heterogenous cell density seeding with some tissue next to the blood vessel. Furthermore, ensuring that the vascularisation occurs early and quickly is important to the success of the tissue viability and growth. This investigation was limited to numerical simulation—no theoretical understanding of the nature of the results was developed.

In this paper, we examine oxygen transport and cell proliferation and migration when the oxygen source is given by a moving vascularisation front. We extend the work of Croll et al. (2005) and Lewis et al. (2005). The additional effects of vascular growth, homogenous and heterogenous seeding, diffusion of cells and critical hypoxic oxygen concentration are considered here. The conditions for the existence of a hypoxic region for a homogenous seeding regime are determined. For the case of heterogenous seeding, the evolution of the cell density and the length of time hypoxic conditions exist are investigated. This theoretical work provides a sound basis and a fundamental understanding of the important interplay between the parameters and allows for a theoretical assessment of a seeding strategy in a vascularising scaffold.

2. Mathematical model

The in vivo scaffold with an A-V loop produces cells and oxygen profiles in three dimensions. Croll et al. (2005) developed a mathematical model in spherical geometry, dependent only on the radial distance. Here, a one-dimensional Cartesian mathematical model is appropriate for exploring the mechanisms involved in cell proliferation and migration on a vascularising scaffold.

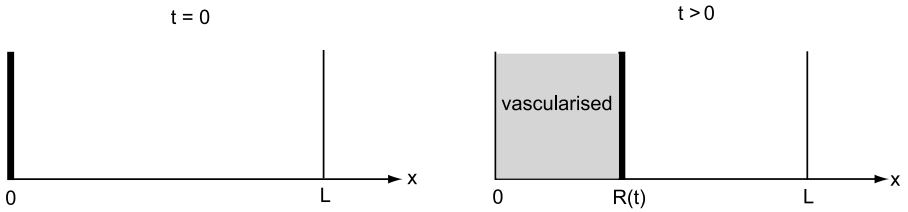

Fig. 2 Schematic diagram of the scaffold $0 < x < L$ at time $t = 0$ and at a later time (some $t > 0$), when the vascularisation front has moved to $R(t)$. The vascularised region is $0 < x < R(t)$, while the avascular region is $R(t) < x < L$.

The scaffold extends from $0 < x < L$, where x denotes the spatial coordinate, as illustrated in Fig. 2. At time $t = 0$, the main blood vessel is at $x = 0$. Over time capillaries grow into the scaffold and penetrate to $x = R(t)$, so that a vascular region extends throughout $0 < x < R(t)$, where $R(0) = 0$. We suppose that oxygen is supplied at a fixed concentration throughout this vascularised region. The far boundary of the scaffold is fixed and insulated, so that there is no diffusive flux of cells or oxygen there. The avascular region of the scaffold is $R(t) < x < L$.

We denote the cell number density by ρ and the local oxygen concentration by c. Following Croll et al. (2005) and Lewis et al. (2005), we suppose that the rate of proliferation of the cells is $\mu(c)$ and that the rate of oxygen consumption per cell is $\alpha\mu(c)$, where α is a constant for low values of cell density. Unlike earlier work, we wish to account for cell crowding in the heterogenous seeding case. A simple way to do this is assume that cells proliferate according to a logistic law (Murray, 2002). We assume that the diffusion coefficients of cells and oxygen are constants D_ρ and D, respectively.

Throughout the scaffold $0 < x < L$, the conservation equation governing the proliferation and diffusion of cells is

$$\frac{\partial \rho}{\partial t} = D_\rho \frac{\partial^2 \rho}{\partial x^2} + \mu(c)\rho\left(1 - \frac{\rho}{\rho_\infty}\right). \tag{1}$$

The appropriate boundary and initial conditions are

$$\frac{\partial \rho}{\partial x}(0, t) = 0, \qquad \frac{\partial \rho}{\partial x}(L, t) = 0, \tag{2}$$

$$\rho(x, 0) = \rho_0 f(x), \tag{3}$$

where ρ_0 is a constant. The form of $f(x)$ is determined by the cell seeding strategy.

In the avascular region of the scaffold is $R(t) < x < L$, the conservation equation governing the transport and consumption of oxygen is

$$\frac{\partial c}{\partial t} = D\frac{\partial^2 c}{\partial x^2} - \alpha\mu(c)\rho. \tag{4}$$

The oxygen diffusion could be modified to account for local cell density, but Croll et al. (2005) found this had negligible effect on the results, and so is ignored here.

In the vascularised region $0 < x < R(t)$, the oxygen concentration is the maximum value, denoted c_∞, everywhere; hence $c(x,t) = c_\infty$ throughout this region. Therefore, the boundary and initial conditions for Eq. (4) are

$$c\big(R(t),t\big) = c_\infty, \qquad \frac{\partial c}{\partial x}(L,t) = 0. \tag{5}$$

$$c(x,0) = c_0, \quad 0 < x < L, \tag{6}$$

where $R(0) = 0$ and c_0 is a constant.

In this model, we have assumed that the position of the vascularisation front is uncoupled from the dynamics of the cell density. Therefore, the position of $R(t)$ must be prescribed. In Section 5, a vascularisation model is presented, which establishes a particular form for $R(t)$.

For convenience and to reduce the number of parameters, we scale all the variables so that a non-dimensional form of the equations can be analysed. Consider

$$\rho = \rho_0\bar{\rho}, \qquad c = c_\infty\bar{c}, \qquad x = L\bar{x}, \qquad t = \frac{1}{\mu(c_\infty)}\bar{t}, \tag{7}$$

$$\mu(c) = \mu(c_\infty)\bar{\mu}(\bar{c}), \qquad \rho_\infty = \rho_0\bar{\rho}_\infty, \qquad c_0 = c_\infty\bar{c}_0, \qquad R = L\bar{R}, \tag{8}$$

and introduce three dimensionless parameters

$$\beta = \frac{D}{L^2\mu(c_\infty)}, \qquad \gamma = \frac{\alpha\rho_0}{c_\infty}, \qquad \delta = \frac{D_\rho}{L^2\mu(c_\infty)}. \tag{9}$$

The parameter β represents the rate of oxygen diffusion relative to the rate of cell proliferation. The parameter γ represents the rate of oxygen consumption relative to the rate of cell proliferation; this parameter increases as the initial cell density ρ_0 increases. The parameter δ represents the rate of cell diffusion relative to the rate of cell proliferation.

The transport equations can now be written in terms of these three non-dimensional parameters. Dropping the overbar notation for convenience, the system of equations and the initial and boundary conditions can be written as

$$\frac{\partial\rho}{\partial t} = \delta\frac{\partial^2\rho}{\partial x^2} + \mu(c)\rho\left(1 - \frac{\rho}{\rho_\infty}\right), \quad 0 < x < 1, \tag{10}$$

$$\frac{\partial c}{\partial t} = \beta\frac{\partial^2 c}{\partial x^2} - \gamma\mu(c)\rho, \qquad R(t) < x < 1, \tag{11}$$

$$c(x,t) = 1, \quad 0 < x < R(t), \tag{12}$$

with $R(0) = 0$ and

$$\rho(x,0) = f(x), \qquad c(x,0) = c_0, \tag{13}$$

$$\frac{\partial\rho}{\partial x}(0,t) = 0, \qquad \frac{\partial\rho}{\partial x}(1,t) = 0, \tag{14}$$

$$c\big(R(t),t\big) = 1, \qquad \frac{\partial c}{\partial x}(1,t) = 0. \tag{15}$$

It is worth noting that in the vascularised region $0 < x < R(t)$, since $c = 1$ everywhere giving $\mu(1) = 1$, the cell density equation (10) reduces to the Fisher equation (Murray, 2002):

$$\frac{\partial \rho}{\partial t} = \delta \frac{\partial^2 \rho}{\partial x^2} + \rho\left(1 - \frac{\rho}{\rho_\infty}\right). \tag{16}$$

2.1. Proliferation rate

The most commonly used functional forms, the linear and the Michaelis–Menten functions, are chosen here to describe the proliferation rate $\mu(c)$. After appropriately scaling to satisfy $\mu(1) = 1$, we write these as

$$\mu(c) = c \quad \text{and} \quad \mu(c) = \frac{c(1+K)}{K+c}, \tag{17}$$

where K is the half-saturation constant. Croll et al. (2005) considered Michaelis–Menten kinetics, Lewis et al. (2005) considered the linear kinetic form. As seen in (17), when the value of K is sufficiently large, the nonlinear Michaelis–Menten law can be well approximated by the linear law.

We are interested in identifying any hypoxic regions inside the seeded scaffold. Here we formally define a hypoxic region to be a region where the oxygen concentration falls below a (dimensionless) hypoxic threshold, denoted c_h. Hence the boundary of the hypoxic region is defined as the position $X(t)$ where

$$c\big(X(t), t\big) = c_h. \tag{18}$$

Certainly for a variety of cell lines (Croll et al., 2005) and for sufficiently small values of the constant K, the nonlinear Michaelis–Menten kinetic law (17) can be well approximated by a much simpler law as follows. In a non-hypoxic region, we let the cell proliferation rate equal a constant with value unity, corresponding to the maximum saturated rate in (17), while in a hypoxic region, where the oxygen concentration falls below c_h, the cell proliferation rate is taken to be zero. Therefore, we write

$$\mu(c) = \mathrm{H}(c - c_h), \tag{19}$$

where $\mathrm{H}(c - c_h)$ is the Heaviside step function. This type of proliferation rate was considered by Lewis et al. (2005). They used the approximation $\mu(c) = \mathrm{H}(c)$ for an avascular scaffold, which was seeded homogenously, while cell diffusivity was neglected.

3. Numerical solution

The position of the vascularisation front $R(t)$ must be prescribed. In Section 5, a vascularisation model, based on a wound-healing angiogenesis model by Pettet et al. (1996a), is presented. There we establish the existence of a vascularisation front that moves at a constant speed. In dimensionless terms, we write

$$R(t) = \lambda t, \tag{20}$$

where the value of λ can be related to the various parameters in the vascularisation model. Such a linear form was used by Croll et al. (2005). Of course, our system could be solved with any prescribed form of $R(t)$ and is not restricted to the linear form.

We now describe two methods for solving the system of equations and conditions for the oxygen concentration and cell density in the vascular and avascular regions (10–15).

3.1. Method 1

We have a partial differential equation for cell density across the whole scaffold. In contrast to this, a partial differential equation defines the oxygen concentration in part of the scaffold only. In this method, we wish to replace the condition $c(x,t) = 1$ in the vascular region $0 < x < R(t)$ with a partial differential equation with solution $c = 1$. We choose to do this in the most simple way by writing

$$\frac{\partial c}{\partial t} = \beta_v \frac{\partial^2 c}{\partial x^2}, \quad 0 < x < R(t), \tag{21}$$

with boundary condition $c(0,t) = 1$. The diffusion constant β_v is chosen to be sufficiently large so that the solution to (21) and (11) over $0 < x < 1$, coupled with (10), gives a solution which approximates $c = 1$ in the vascular region, and in particular $c(R(t),t) = 1$ in equation (15). (In our examples, $\beta_v = 10^3\beta$ was found to be sufficient.) Note that the consumption of oxygen in this region is balanced by the oxygen source due to the evolving vascularisation.

These equations are solved using the parabolic solver D03PCF from NAG Fortran Library routine. This numerical method ensures that the cell density and cell flux, as well as the oxygen concentration and oxygen flux, are continuous across $R(t)$, the boundary between the vascular and avascular regions.

3.2. Method 2

Here we solve the system of partial differential equations for ρ and c, namely (10–11), in the avascular region $R(t) < x < 1$. Then we require a boundary condition for ρ at $x = R(t)$. We choose a zero-flux boundary condition $\frac{\partial \rho}{\partial x}(R(t),t) = 0$. Then the solution in the avascular region can be numerically determined, independent of the solution in the vascular region. The partial differential equations describing the cell population density and oxygen concentration in the avascular region $R(t) < x < 1$ is a moving boundary problem. The partial differential equations for ρ and c can be transformed to fixed boundary problems, as outlined in Appendix A. The resulting equations are solved using the parabolic solver D03PCF from NAG Fortran Library routine.

To obtain an approximation to the solution in the vascular region $0 < x < R(t)$, we assume that cell proliferation dominates over the cell migration term in this region. This assumption is excellent for the homogenous seeding case only, but is inappropriate for the heterogenous case—we comment on this in Section 4. Then the equation describing the cell density in the vascularised region (16) is well-approximated by

$$\frac{\partial \rho}{\partial t} = \rho\left(1 - \frac{\rho}{\rho_\infty}\right). \tag{22}$$

Table 1 Parameter values derived from Croll et al. (2005)

Maximum oxygen concentration c_∞	80 nmol/ml
Maximal cell growth rate $\mu(c_\infty)$	5×10^{-6} s^{-1}
Oxygen uptake rate α	20 cells/mol
Michaelis–Menten half-saturation constant K	4.0 nmol/ml
Diffusion rate of cells D_ρ	5×10^{-9} cm^2/s
Diffusion rate of oxygen D	3×10^{-5} cm^2/s
Speed of capillary front Γ	0.05 cm/day
Distance from main vessel to outer edge of scaffold L	0.5 cm
Hypoxic limit of oxygen concentration c_h	5 nmol/ml
Initial oxygen concentration c_0	8 nmol/ml
Carrying capacity ρ_∞	5×10^8 cells/ml
Initial cell density: homogeneous seeding ρ_0	5×10^5 cells/ml
Initial cell density: heterogeneous seeding ρ_0	5×10^8 cells/ml
Initial width of cell seeding: heterogeneous seeding $\tilde{x}$	0.03 cm

The cell density must be continuous at the vascularisation boundary $R(t)$. We denote $N(t)$ to be the value of $\rho(R(t)^+, t)$ determined from the numerical solution in the avascular region. Then it follows that the cell density in the vascular region is just

$$\rho(x,t) = \frac{\rho_\infty N(\frac{x}{\lambda}) e^{(t-\frac{x}{\lambda})}}{\rho_\infty + N(\frac{x}{\lambda})(e^{(t-\frac{x}{\lambda})} - 1)}, \quad 0 < x < R(t). \tag{23}$$

The x/λ is the time when location x first becomes vascularised. For a more general $R(t)$, the term x/λ must be replaced by $R^{-1}(x)$.

3.3. Parameter values

The choice of parameters, listed in Table 1, is based on the extensive literature search conducted by Croll et al. (2005), where references are provided. The cell seeding strategy determines the initial condition. Both homogenous and heterogenous cell seeding conditions are considered.

4. Results

The evolution of the cell density and oxygen concentration to homogenous and heterogenous cell seeding initial conditions is now considered. Both numerical and theoretical results are presented.

4.1. Homogenous seeding

To obtain an initial uniform low density distribution of cells, the scaffold is soaked in a solution containing cells. For this case the initial cell density is very much lower than the theoretical maximum cell density. The initial condition for the cell density will be

$$\rho(x,0) = f(x) = 1. \tag{24}$$

Using the parameter values in Table 1, the dimensionless quantities are approximately $\beta = 20$, $\gamma = 200$, $\delta = 0.001$, $\lambda = 0.2$, $\rho_\infty = 1{,}000$ and $K = 0.05$.

Figure 3 presents the oxygen concentration and cell density profiles as a function of position at increasing times, as well as oxygen concentration and cell density profiles as a function of time, for several fixed positions in the scaffold. Three functional forms for the cell proliferation rate—linear, Michaelis–Menten and step function—are investigated. In all cases, the oxygen concentration decreases across the scaffold, with the highest level at the vascularisation front. These profiles essentially preserve their shape and move across the region with time, as the vascularisation front moves into the scaffold. The cell density increases throughout, but much more rapidly in the vascularised region or close to it. This gives rise to a heterogenous distribution of cells evolving throughout the scaffold. In a hypoxic region, the cell proliferation is insignificant.

When $\mu(c) = c$ (equivalent to large K limit), the cell proliferation is significantly reduced compared to the other two cases, resulting in a smaller cell density throughout; moreover, for the parameter values chosen here, a hypoxic region is absent. For the Michaelis–Menten and step function form of $\mu(c)$, the oxygen concentration immediately falls below the hypoxic concentration in the right side of the scaffold, and hence a hypoxic region develops. Since the scaffold is homogenously seeded, all the cells in the hypoxic region are subject to insufficient levels of oxygen. For this set of parameter values, the hypoxic region retreats as the vascularisation front moves into the scaffold, as seen in the Fig. 3(e).

However, for larger values of β/γ, the hypoxic region can initially increase in width, since those cells close to the vascularised region are proliferating and therefore consuming increased levels of oxygen. However, since the vascularisation region is moving into the scaffold, there is a time where the hypoxic region begins to decrease in size; it will eventually disappear, as illustrated in Fig. 4 and discussed further in Appendix B. This behaviour is quite different from the non-vascularising case illustrated in Fig. 1.

For the homogenous seeding case, the results of the two numerical methods described in Sections 3.1 and 3.2 are almost identical for the linear and step function forms of $\mu(c)$ cases and are approximately the same for the Michaelis–Menten case. The results presented were obtained using Method 1.

4.1.1. Some analytical results derived from the step function form of $\mu(c)$

Comparison of the corresponding graphs in the central and right columns of Fig. 3 show that the respective c and ρ profiles, as well as the hypoxic region, are very similar. Hence the step function form of the proliferation rate is a good approximation for the Michaelis–Menten form, since K is sufficiently small. When the relative rate of oxygen consumption to cell proliferation, given by γ, is sufficiently large, the oxygen concentration equation is effectively in a pseudo-steady state. Consequently, with the step function form of $\mu(c)$ the equations can be sufficiently simplified to admit some analytical solutions, at least for early times, for the homogenous seeding case. We summarise these findings here; the details of the analysis are outlined in Appendix B.

We first define W as

$$W = \frac{2\beta}{\gamma}(1 - c_h), \tag{25}$$

a parameter that depends on the ratio of the oxygen diffusion rate and oxygen consumption rate and the non-hypoxic oxygen concentration range.

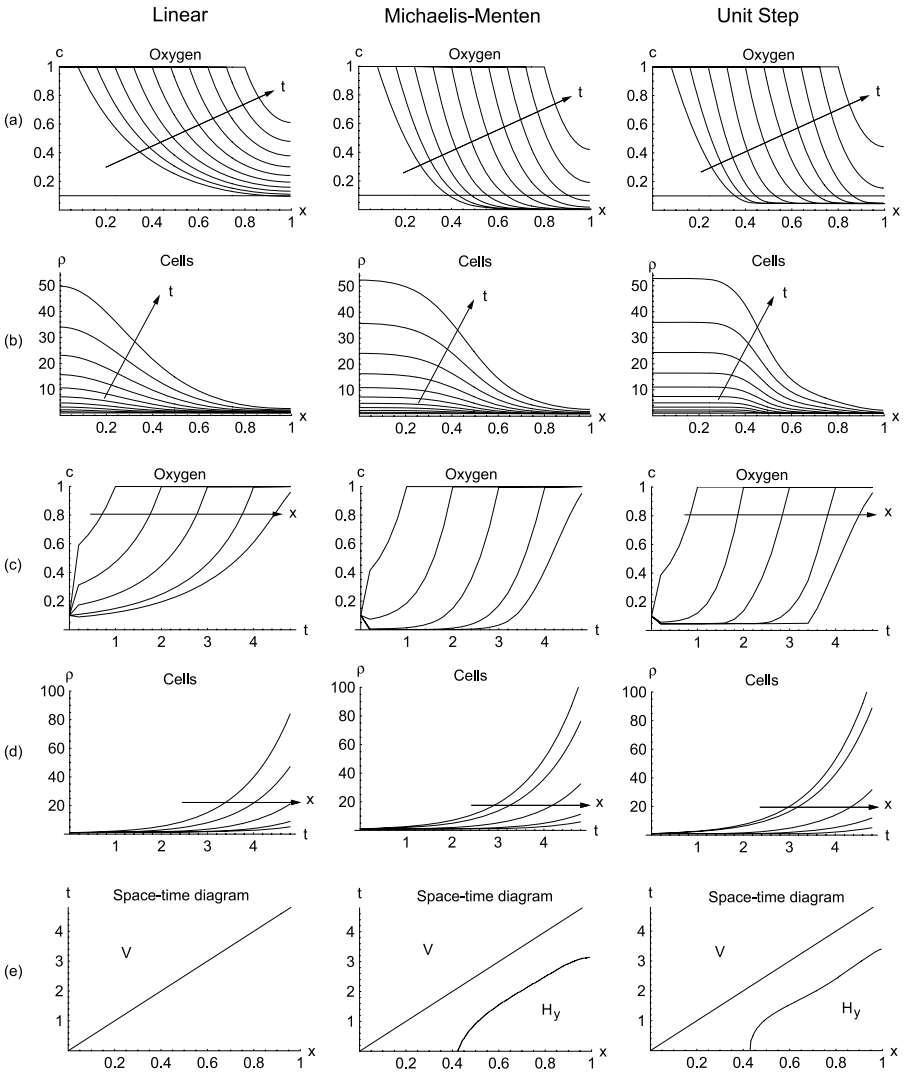

Fig. 3 Homogenous seeding: Oxygen concentration profiles, cell density profiles and space time diagram with $R(t) = \lambda t$. Left column: Linear $\mu(c) = c$. Central column: Michaelis–Menten $\mu(c) = c(1+K)/(K+c)$ with $K = 0.05$. Right column: Step function $\mu(c) = \mathrm{H}(c - c_h)$ with $c_h = 0.05$. Rows (a) and (b): Oxygen concentration $c(x,t)$ for $t = 0, 0.4, 0.8, \ldots, 3.6, 4.0$ and cell density $\rho(x,t)$ versus x for $t = 0, 0.4, 0.8, \ldots, 3.2$. Arrows indicate increasing t profiles. Rows (c) and (d): Oxygen concentration $c(x,t)$ and cell density $\rho(x,t)$ versus t for $x = 0.2, 0.4, 0.6, 0.8, 1.0$. Arrows indicate increasing x profiles. Row (e): Space-time diagram indicating the vascularised and any hypoxic regions. V denotes the vascularised region, while $\mathrm{H_y}$ denotes a hypoxic region. For all cases, $\beta = 20, \gamma = 200, \delta = 0.001, \lambda = 0.2, c_h = 0.05, c_0 = 0.1, \rho_\infty = 1000, f(x) = 1$.

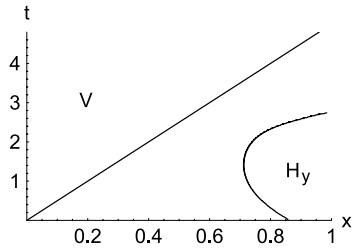

Fig. 4 Typical space time diagram for a sufficiently large value of β/γ with homogenous seeding. The hypoxic region initially increases in size, but eventually retreats with time. V denotes the vascularised region, while H_y denotes a hypoxic region.

When $W < 1$, then a hypoxic region is established right from the start, as seen in the right column in Fig. 3(e), where $W = 0.095$. Then the hypoxic region is $X(t) < x < 1$, where the position of the hypoxic front $X(t)$ is defined as $c(X(t), t) = c_h$, from Eq. (18). We can estimate the initial width of the hypoxic region as

$$X(0) = \sqrt{W}. \tag{26}$$

For our example, this gives $X(0) = 0.44$, which approximates well the position illustrated in Fig. 3(e). For this example, the width of the avascular, non-hypoxic region $R(t) < x < X(t)$ remains approximately constant and is given by $X(t) - R(t) \approx X(0)$. Therefore, applying the approximation $X(t) \approx \lambda t + X(0)$, we can estimate the length of time t_H that a fixed position x is under hypoxic conditions, as

$$t_H = \frac{1}{\lambda}\left(x - \sqrt{W}\right). \tag{27}$$

When $W > 1$, then there is no hypoxic region at the start. However two possible cases emerge at a later time; namely, a hypoxic region develops at some time, or a hypoxic region never develops. In the first case, there will exist an initial period of time where there is no hypoxic region. After this initial phase, a hypoxic region develops from the far end of the scaffold. In the second case, if the vascularisation front moves in sufficiently rapidly, no hypoxic region develops at any time.

Therefore, the existence of a hypoxic region depends on a balance between the speed of the vascularisation front λ and the parameter W. This is clearly illustrated in the bifurcation diagram Fig. 5. The solid line defines the boundary between the existence and absence of any hypoxic region; this line is defined by the transcendental equation

$$2\lambda e^{\frac{1}{2\lambda}-1} - \sqrt{W} = 0. \tag{28}$$

Upper and lower bounds can be determined using asymptotics as

$$2\lambda = \frac{1}{1 + \frac{1}{2}\ln W + \ln\left(1 + \frac{1}{2}\ln W\right)}, \quad \text{for } W \to \infty, \tag{29}$$

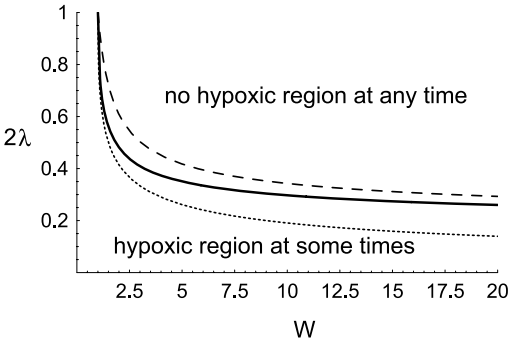

Fig. 5 Bifurcation diagram of 2λ versus $W = \sqrt{2\beta(1-c_h)/\gamma}$. The solid line separates the regions of parameter space where a hypoxic region exists at some time or not at all. Here $R(t) = \lambda t$. The asymptotic approximations for $W \to \infty$ (long dashed line), given by (29), and $W \to 1$ (dotted line), given by (30), are shown.

and

$$2\lambda = \frac{1}{1+\sqrt{2(W-1)}}, \quad \text{for } W \to 1. \tag{30}$$

These are good approximations as shown in Fig. 5.

4.2. Heterogenous seeding

Rather than soaking a scaffold to obtain an initial uniform low density distribution of cells, a small biopsy of tissue can be placed adjacent to the blood vessel. This produces heterogenous seeding. For this case the initial cell density is approximately equal to the theoretical maximum cell density. Now the value of ρ_0 in the parameter γ will be much larger than in the homogenous seeding case (three orders of magnitude as seen in Table 1). The initial condition for the cell density will be

$$\rho(x,0) = f(x) = \mathrm{H}(\tilde{x} - x), \tag{31}$$

where $\tilde{x}$ is chosen to be small.

Using the parameter values in Table 1, the dimensionless quantities are approximately $\beta = 20$, $\gamma = 180{,}000$, $\delta = 0.001$, $\lambda = 0.2$, $\rho_\infty = 1.111$ and $K = 0.05$.

For this case, the consumption rate of oxygen is so large locally near the left boundary that the oxygen concentration drops from $c = 1$ to $c = 0$ in a very narrow region there. Consequently, except for a narrow region at the vascularisation front, almost the whole scaffold is hypoxic. For early times, this profile moves into the scaffold at the vascularisation rate λ. Meanwhile over this short time period the cells diffuse to the right, but the density drops rapidly to zero since there is no oxygen to sustain proliferation. For this case, the approximate time for the vascularisation front to move past the bulk of cells is $\tilde{x}/\lambda$. After this time, the bulk of the cells has access to the maximum value of the oxygen concentration, and therefore no hypoxic region exists. Thereafter, the cell growth is governed by the Fisher equation (16). The cell density profiles evolve to a travelling wave,

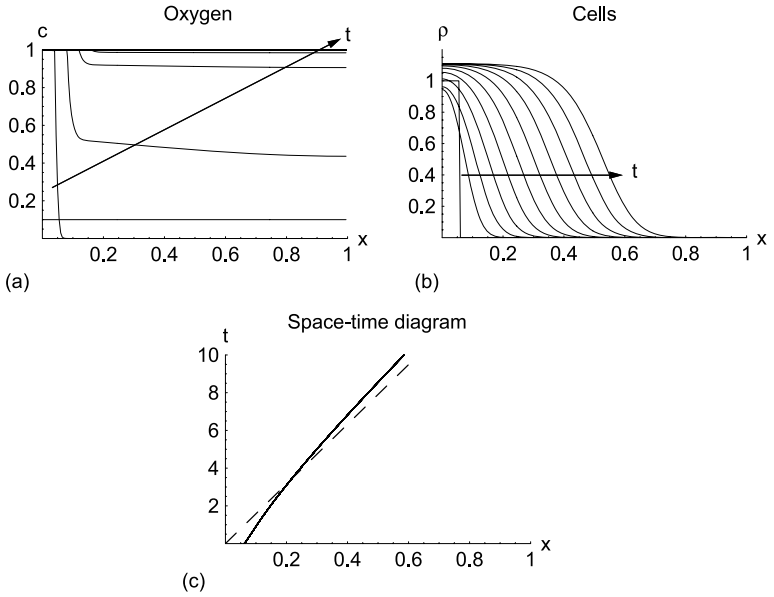

Fig. 6 Heterogenous seeding: Oxygen and cell density profiles as a function of x with $R(t) = \lambda t$. (a) Oxygen profile at $t = 0, 0.2, 0.4, \ldots, 4.0$. (b) Cell density profile at $t = 0, 1, 2, \ldots, 9, 10$. Here $\mu(c) = c(1 + K)/(K + c)$ with $K = 0.05$, $\beta = 20$, $\gamma = 180{,}000$, $\delta = 0.001, \lambda = 0.2, c_0 = 0.1, \rho_\infty = 1.111$, $\tilde{x} = 0.06$. Arrows indicate increasing t profiles. (c) Space-time diagram indicating the contour where $\rho(x, t) = 0.25$ (solid line) to the line $x = 2\sqrt{\delta}$ (dashed line). The slopes become approximately parallel, providing a wave speed for the density wave.

as shown in Fig. 6(b). The travelling wave preserves its shape and moves across the domain with an almost constant speed. The Fisher wave, as determined from semi-compact support initial conditions, evolves to a wave moving with dimensionless wave speed of $2\sqrt{\delta}$ (Murray, 2002). The speed of our density profiles can be estimated by tracking a particular density contour (here $\rho(x, t) = 0.25$), as illustrated in Fig. 6(c). After an initial time period for the wave to establish, the slope of the contour approaches this theoretically determined value.

Hence the condition $2\sqrt{\delta} < \lambda$ ensures that the cell population is behind the vascularisation front for all time after an initial time period.

For the chosen parameter values, the cell population density travels with wave speed $2\sqrt{\delta} = 0.06$, which is significantly slower than the vascularisation speed $\lambda = 0.2$. The oxygen profiles are very dependent on the value of λ, as shown in Fig. 7, where two cases $\lambda = 0.2$ and $\lambda = 0.1$ are shown. However, the cell densities looked little different for the two cases, and therefore, are not illustrated here.

After the vascularisation front moves past the bulk of cells, the oxygen concentration increases in the avascular region, and is approximately equal to unity everywhere, since the oxygen consumption is low due to the insignificant cell numbers. Therefore, the oxygen profiles are constant over much of the domain.

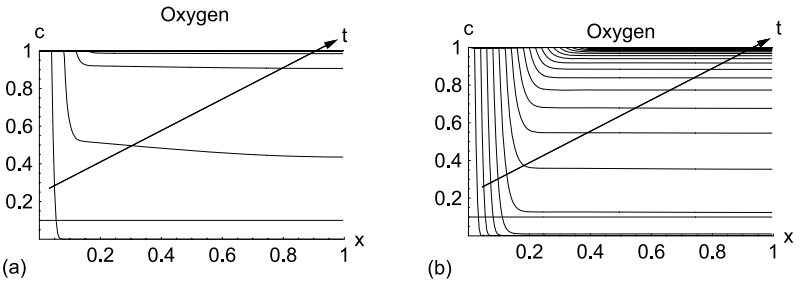

Fig. 7 Heterogenous seeding: Oxygen profiles as a function of x with $R(t) = \lambda t$. (a) Faster vascularisation: $\lambda = 0.2$. (b) Slower vascularisation: $\lambda = 0.1$. Here $\mu(c) = c(1+K)/(K+c)$ with $K = 0.05$ for $t = 0, 0.2, 0.4, \ldots, 4$. $\beta = 20$, $\gamma = 180{,}000$, $\delta = 0.001$, $c_0 = 0.1$, $\rho_\infty = 1.111$, $\tilde{x} = 0.06$. Arrows indicate increasing t profiles.

Hence, if λ is sufficiently large, the cell density profiles are governed by a balance of migration and proliferation behind the vascularisation front, as given by Fisher's equation. In terms of dimensioned variables, the speed of cell migration is governed by $2\sqrt{D_\rho \mu(c_0)}$.

For the heterogenous seeding case, the diffusion of cells in the vascular region is important. The numerical Method 2 described in Section 3.2 cannot produce the physically expected local decrease in the cell density near $x = 0$ for early times. Therefore, these results were obtained using Method 1 in Section 3.1.

5. Vascularisation model to establish the form of $R(t)$

Here we outline a vascularisation model, adapted from a wound-healing angiogenesis model of Pettet et al. (1996a). The model is shown to support travelling wave solutions, which gives rise to a vascularisation front that moves linearly with time.

The development of vascularisation requires the formation of new blood vessels (angiogenesis). Chemical stimuli, called angiogenic factors, are placed inside the scaffold to promote the formation of buds or capillary tips on blood vessels. Such a process, in a different context, has been modelled using the density of capillary tips, n, the concentration of angiogenic factors, called attractants a, and the density of blood vessels, b (Balding and McElwain, 1985; Pettet et al., 1996a, 1996b).

Following the methods of Pettet et al. (1996a), we write down conservation equations for each of the species. We assume that space and time have already been scaled with the same parameters as previously, and so all variables here are dimensionless. The system of equations is

$$\frac{\partial n}{\partial t} = \mu_n \frac{\partial^2 n}{\partial x^2} - \chi \frac{\partial}{\partial x}\left(n \frac{\partial a}{\partial x}\right) + \kappa_1 ab - \kappa_2 n^2, \tag{32}$$

$$\frac{\partial a}{\partial t} = -\kappa_3 ab, \tag{33}$$

$$\frac{\partial b}{\partial t} = \mu_b \frac{\partial}{\partial x}\left(n \frac{\partial b}{\partial x}\right) - \mu_n \frac{\partial n}{\partial x} + \chi n \frac{\partial a}{\partial x}. \tag{34}$$

The flux of capillary tips is governed by a random motility and a chemotactic migration term due to the presence of attractants. In the presence of attractants, capillary tips develop from blood vessels due to budding. The dominant mechanism of capillary tip decay is assumed to be the merging of tips (anastomosis). Here, the equation for the attractant is different from the one used in Pettet et al. (1996a). Instead of the attractant being produced in the wound space, the attractant is now initially present in the scaffold; the attractant is assumed to be immobile and to degrade as new blood vessels are formed. The blood vessels are assumed to have a flux due to the presence of capillary tips, modelled by a nonlinear flux term of blood vessels. Moreover, as the capillary tips move, a trail of new vessels is assumed to be produced at a rate which depends on the flux of capillary tips, giving the snail trail effect (Edelstein, 1982; Pettet et al., 1996a). Here μ_n and μ_b are the random motility coefficients, χ is the chemotaxis coefficient, κ_1 is the rate of budding of capillary tips in the presence of attractants, κ_2 is the decay rate of capillary tips due to merging and κ_3 is the decay rate of the attractants in the presence of blood vessels.

At time $t = 0$, we start with initial budding of the main vessel due to the presence of a uniform concentration of attractant:

$$n(x,0) = \mathrm{H}(x-h), \qquad a(x,0) = 1, \qquad (x,0) = \hat{b}\mathrm{H}(x-h). \tag{35}$$

The boundary conditions are chosen as

$$\frac{\partial n}{\partial x}(0,t) = 0, \qquad \frac{\partial a}{\partial x}(0,t) = 0, \qquad b(0,t) = \hat{b}, \tag{36}$$

$$\frac{\partial n}{\partial x}(1,t) = 0, \qquad \frac{\partial a}{\partial x}(1,t) = 0, \qquad \frac{\partial b}{\partial x}(1,t) = 0. \tag{37}$$

Figure 8 illustrates profiles of the capillary tip density, attractant concentration and blood vessel density at regular time intervals. The model gives rise to travelling wave profiles, with a narrow peak of capillary tips ahead of the developed blood vessels that are degrading the chemical attractant. Typical wave profiles are shown in Fig. 9(a). A blood vessel network develops and moves into the scaffold, with capillary tips at the leading edge, where there is a significant attractant gradient. These profiles move with a constant speed. Since there is a marked transition region in the profiles, a travelling wave boundary layer analysis is useful to provide a relationship between the wave speed and the parameters of the system. As outlined in Appendix C, we seek solutions

$$N(z) = n(x,t), \qquad A(z) = a(x,t), \qquad B(z) = b(x,t), \tag{38}$$

in terms of a travelling wave co-ordinate $z = x - st$, where s is the wave speed. The wave speed can be identified as the speed of the vascularisation front.

Introducing a new parameter

$$\Psi = \frac{\chi}{3s}\sqrt{\frac{\kappa_1}{\kappa_2}}, \tag{39}$$

the asymptotic behaviour of the solution is

$$N = \sqrt{\frac{\kappa_1}{\kappa_2}AB}, \qquad B = \Psi^2\left(1 - A^{\frac{3}{2}}\right)^2, \tag{40}$$

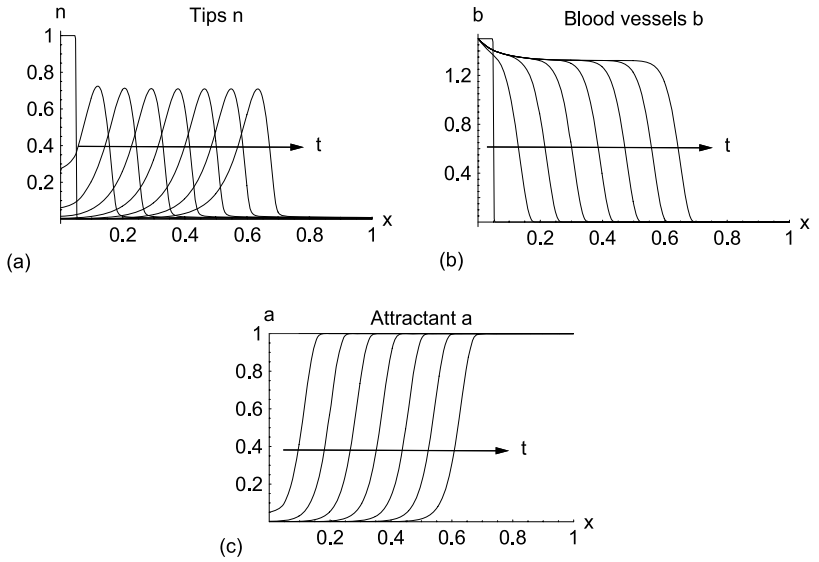

Fig. 8 Profiles of capillary tips, blood vessels and attractant at regular time intervals. (a) Capillary tips $n(x,t)$. (b) Blood vessels $b(x,t)$. (c) Attractant $a(x,t)$. Here $\mu_n = 0.001$, $\mu_b = 0.001$, $\kappa_1 = 1000$, $\kappa_2 = 1000$, $\kappa_3 = 1$, $\hat{b} = 1.5$, $h = 0.05$. Profiles are plotted at times $t = 0, 2, 4, \ldots, 12, 14$. Arrows indicate increasing t profiles.

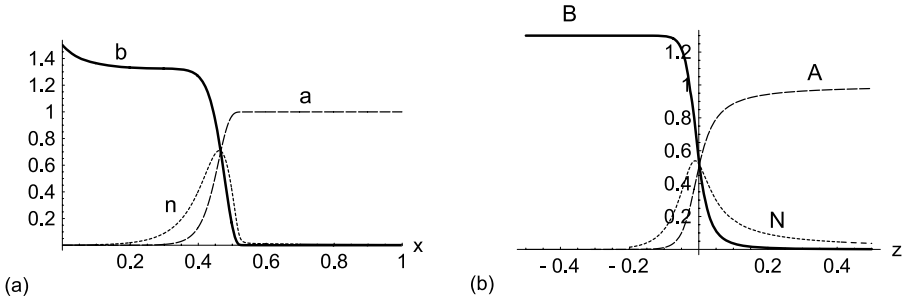

Fig. 9 Typical wave profiles of capillary tips, blood vessels and attractant at a fixed time. (a) Numerical solutions as in Fig. 8. (b) Asymptotic travelling wave solutions N, B, A from a boundary layer analysis as a function of the travelling wave co-ordinate z.

$$\frac{dA}{dz} = \frac{\kappa_3}{s} A\left\{\Psi\left(1 - A^{\frac{3}{2}}\right)\right\}^2. \tag{41}$$

A relationship between the wave speed s and vascularised density of blood vessels $b_{-\infty}$ can be established as

$$s = \frac{\chi}{3\sqrt{b_{-\infty}}}\sqrt{\frac{\kappa_1}{\kappa_2}}. \tag{42}$$

The typical profiles for n, a, b in Fig. 9(a) can be compared to the asymptotic form of N, A and B as a function of the travelling wave coordinate z in Fig. 9(b). Certainly Fig. 9(b) has some qualitative similarities to the wave profile Fig. 9(a). The computed wave speed of the solutions in Fig. 8 is $s \approx 0.04$, whereas with $b_{-\infty} = 1.3$, the approximation (42) gives $s \approx 0.03$. Choosing different parameter values also produces differences in the numerical wave speed to that calculated by (42), as also observed in (Pettet et al., 1996a). The decay parameter κ_3 does not appear in the wave speed, but only in shape of the solutions. However, on computing numerical solutions, some dependence on this parameter is observed.

We have presented a simple model for the development of a blood vessel network which travels with constant speed, s, across the scaffold. The interface between the blood vessels and tips and the avascular region is approximated in Section 2 by a sharp boundary defined as $R = \lambda t$. This model motivates the use of $R = \lambda t$ for the position of the vascularisation front; in fact both s and λ are identified with the speed of the front.

6. Discussion

Hypoxic conditions inside a scaffold reduce the efficacy of tissue engineering applications. Since it is difficult to measure oxygen levels in vivo, simulations of the oxygen profiles and cell density using a mathematical model provides a powerful tool for understanding whether a certain seeding strategy will be successful in producing viable tissue.

We develop a simple model for capillary growth, due to effects of chemical stimuli alone, which considers capillary tips, a depleting attractant chemical stimuli based within the scaffold and blood vessels, based on Pettet et al. (1996a, 1996b). The model supports travelling wave profiles, with a narrow vascularisation front of capillary tips ahead of developed blood vessels degrading the attractants. The system can be simplified using travelling wave boundary layer analysis, so yielding an approximation to the constant wave speed based on vascularised density of blood vessels and ratio of capillary tip growth and decay. These results motivate our chosen form for the position of vascularisation front, one which moves linearly in time.

Our model of oxygen concentration and cell proliferation and migration inside such a vascularising scaffold is used to investigate and assess the differences in alternate functional forms for the consumption rates of oxygen (linear, Michaelis–Menten and simple step-functional form).

With homogenous seeding and parameter values relevant to our application, the Michaelis–Menten model can be well approximated by the step functional form. This simpler form is amenable to some interesting analytical work, which provides a fundamental understanding of the competition between the various processes. Two important dimensionless parameters are determined, namely the dimensionless speed of the vascularisation front λ and the rate at which oxygen diffuses relative to the rate it is consumed and the non-hypoxic oxygen concentration range $W = \sqrt{2\beta/\gamma}(1 - c_h)$. A functional relationship between λ and W establishes whether no hypoxic region exists at any time or whether a hypoxic region exists at some time. Furthermore, if a hypoxic region exists right from the start, an estimate for the time that a fixed position is under hypoxic conditions is determined. The width of the avascular non-hypoxic region has been found to decay for early times, which generalises the results of Lewis et al. (2005).

This provides an important assessment of the time that cells are exposed to hypoxic conditions. To illustrate the spatial and temporal location of the hypoxic region, a useful tool is a space-time diagram showing the vascularised region and hypoxic region.

With heterogenous seeding, a small high density piece of tissue is placed adjacent to the blood vessel. The scaffold will only be non-hypoxic if the bulk of the proliferating and migrating cell population is behind the vascularisation front for most of the time. Hence, we require the vascularisation speed to be faster than the Fisher-like travelling wave of cells, that is $\lambda > 2\sqrt{\delta}$, where δ is the rate of cell diffusion relative to the rate of cell proliferation. An estimate of the length of time that hypoxic conditions exist is given. After this time, there will be sufficient oxygen throughout the scaffold to support the total cell population.

This study has provided important criteria necessary for predicting whether a region will be established where the oxygen concentration falls below a hypoxic threshold. If a hypoxic region is created, then the length of time a position is subjected to these undesirable conditions has been determined. Heterogenous seeding appears to be the only viable way to reduce the hypoxic conditions. In this case, it is most important for the vascularisation front to move into the scaffold sufficiently rapidly. Hence, a thorough understanding of the necessary conditions for early and sufficiently rapid establishment of the vascularisation network is critical to a successful outcome in soft tissue engineering.

Acknowledgements

The authors gratefully acknowledge the support from the ARC Discovery Grant DP0557990. Kerry Landman wishes to thank the Particulate Fluids Processing Center, an Australian Research Council ARC Special Research Center, for support. The authors also wish to thank Dr. Tristan Croll, Prof. Justin Cooper-White and Dr. Mat Simpson.

Appendix A Transformation of the system in the avascular region to a fixed domain

We demonstrate how the differential equations (10–11) defined on $R(t) < x < 1$ can be transformed to one with fixed boundaries. Introduce a new space variable

$$y = \frac{x - R(t)}{1 - R(t)}. \tag{A.1}$$

The left boundary $x = R(t)$ corresponds to $y = 0$, while the right boundary $x = 1$ corresponds to $y = 1$.

Using this transformation, Eqs. (10–11) need to be written in the following form for NAG Library:

$$\frac{\partial \rho}{\partial t} = \frac{\partial}{\partial y}\left(\frac{\delta}{(1-R)^2}\frac{\partial \rho}{\partial y} + \frac{dR}{dt}\frac{1}{1-R}(1-y)\rho\right) + \mu(c)\rho\left(1 - \frac{\rho}{\rho_\infty}\right) + \frac{dR}{dt}\frac{1}{1-R}\rho, \tag{A.2}$$

$$\frac{\partial c}{\partial t} = \frac{\partial}{\partial y}\left(\frac{\beta}{(1-R)^2}\frac{\partial c}{\partial y} + \frac{dR}{dt}\frac{1}{1-R}(1-y)c\right) - \gamma\mu(c)\rho + \frac{dR}{dt}\frac{1}{1-R}c, \tag{A.3}$$

for solution on $0 < y < 1$. The zero-flux boundary conditions for the density at $y = 0$ and both density and oxygen concentration at $y = 1$, as well as the fixed oxygen concentration at $y = 0$, become

$$c = 1, \quad \frac{\delta}{(1-R)^2}\frac{\partial \rho}{\partial y} = -\frac{dR}{dt}\frac{1}{1-R}\rho \quad \text{at } y = 0 \tag{A.4}$$

$$\frac{\partial c}{\partial y} = \frac{\partial \rho}{\partial y} = 0 \quad \text{at } y = 1. \tag{A.5}$$

Appendix B Simplified mathematical model for homogenous seeding

From Fig. 3, we observe that the essential features of our numerical results for Michaelis–Menten kinetics can be captured with a simplified model, using the step function (19). Therefore, we analyse the model with the step function kinetics.

Further simplifications to the equations can be made. Since the initial cell density is far from its carrying capacity, the logistic growth term can be linearised. Furthermore, since $\gamma \gg 1$ and $\beta \gg 1$, Eq. (11) can be approximated by its steady state form. Using all these simplifications, the oxygen equation becomes

$$\frac{\beta}{\gamma}\frac{\partial^2 c}{\partial x^2} - \rho \mathrm{H}(c - c_h) = 0, \tag{B.1}$$

together with boundary conditions (15). The initial condition for c is no longer required. Finally, since the cell diffusivity is small ($\delta \ll 1$), we simplify the cell equation as

$$\frac{\partial \rho}{\partial t} = \rho \mathrm{H}(c - c_h). \tag{B.2}$$

The system (B.1–B.2) is only loosely coupled, and some progress can be made solving these analytically, at least for early times.

There are several cases to consider, depending on whether there is an initial time period when the oxygen concentration remains above the hypoxic level or not. This is determined by the magnitude of $W = 2\beta(1 - c_h)/\gamma$ defined in (25).

B.1 Case $W > 1$

Suppose that for an initial time period the oxygen concentration is greater than the critical value c_h everywhere. Then solving from (B.1–B.2) in the region $R(t) < x < 1$, the cell density and oxygen concentration are given by

$$\rho = e^t \quad \text{and} \quad c = \frac{e^t}{\beta/\gamma}\left(\frac{x^2}{2} - x\right) - \frac{e^t}{\beta/\gamma}\left(\frac{R^2}{2} - R\right) + 1. \tag{B.3}$$

Then $c(1,t) > c_h$ and no hypoxic region exists for those times satisfying

$$e^t\big(1 - R(t)\big)^2 < W. \tag{B.4}$$

Since $R(0) = 0$, this condition only holds at $t = 0$ when $W > 1$. For very rapid vascularisation (that is, sufficiently large dR/dt), and/or sufficiently slow oxygen consumption, $R(t)$ will reach the far boundary while the inequality (B.4) holds; then the domain will never sustain hypoxic conditions. For this case the solutions (B.3) are valid for all time, giving a homogenous distribution of cells, until the whole region is vascularised.

Alternatively, there will exist a critical time τ when the hypoxic region starts evolving from the right hand boundary. This time τ is the solution to

$$e^\tau\big(1 - R(\tau)\big)^2 = W. \tag{B.5}$$

For the case $R(t) = \lambda t$, Fig. 5 illustrates a relationship between λ and W which defines conditions for such a τ to exist.

When such a τ exists, for $t > \tau$, there is a region $X(t) < x < 1$, where the oxygen concentration remains at the hypoxic value c_h, since the cells neither consume oxygen nor proliferate there. In this case, the equations determining c in the non-hypoxic region $R(t) < x < X(t)$ require continuity of concentration and flux at the hypoxic interface $X(t)$. The unknown moving boundary $X(t)$ can be determined from the condition $c(X(t),t) = c_h$. For times $t > t_h$ such that $dX/dt < 0$, the solutions are given by

$$c = \begin{cases} \dfrac{e^t}{\beta/\gamma}\left(\dfrac{x^2}{2} - Xx\right) - \dfrac{e^t}{\beta/\gamma}\left(\dfrac{R^2}{2} - XR\right) + 1, & R < x < X, \\ c_h, & X < x < 1, \end{cases} \tag{B.6}$$

$$\rho = \begin{cases} e^t, & 0 < x < X, \\ e^{t_h} \quad \text{or} \quad N(x), & X < x < 1, \end{cases} \tag{B.7}$$

where the function $t_h(x)$ is the time when the oxygen concentration first falls to c_h at position x defined implicitly by $X(t_h) = x$ or $N(X(t)) = e^{t_h}$. For the case when $R(t) = 0$ this gives $e^{t_h} = N(x) = W/x^2$.

The position $X(t)$ where the oxygen concentration equals c_h is determined by

$$X(t) = R(t) + \sqrt{W}e^{-t/2}. \tag{B.8}$$

Lewis et al. (2005) considered the case $W > 1$, when $R(t) = 0$ for all $t > 0$ and $c_h = 0$. Our results collapse to the ones found in that work, giving the time when the hypoxic region develops as $\tau = t_h(1) = \ln W$.

For our case, X starts at the far boundary ($X(\tau) = 1$ where $\tau > \ln W$) and moves into the scaffold. However, as the vascularisation front continues to move to the right into the scaffold, at some time the hypoxic wavefront $X(t)$ will no longer continue to move to the left into the scaffold ($dX/dt < 0$) and it will begin to move to the right ($dX/dt > 0$). Hence there is a turning point where $dX/dt = 0$, at time $t = \ln[W/(4\lambda^2)]$. After this time the equation governing c becomes more mathematically complex since the density at a position which was once hypoxic and then becomes non-hypoxic now depends on position as well as time. Thus the inhomogeneity in the oxygen equation is now dependent on a

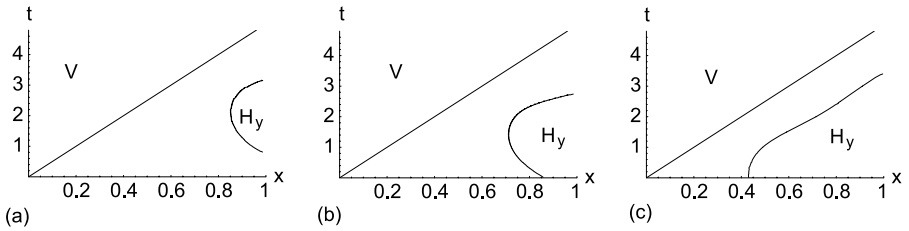

Fig. B.10 Space time diagram for the simplified model with homogenous seeding, illustrating the boundary between the hypoxic and non-hypoxic regions, $X(t)$, and the vascularisation front $R(t)$. (a) $W > 1$ (using $\beta/\gamma = 0.8$ and $c_h = 0.05$). (b) $W < 1$ and $W/(4\lambda^2) > 1$ (using $\beta/\gamma = 0.4$ and $c_h = 0.05$). (c) $W < 1$ and $W/(4\lambda^2) < 1$ (using $\beta/\gamma = 0.1$ and $c_h = 0.05$). V denotes the vascularised region, while H_y denotes a hypoxic region. For all cases, $R(t) = \lambda t$, $\beta = 20, \lambda = 0.2, c_h = 0.05, \delta = 0.001$. These figures have been generated numerically (Method 1 and Method 2 give identical results)—the analytical expression for $X(t)$ when $dX/dt < 0$ matches exactly with the numerically generated results.

density $\rho(x,t)$ ((B.1), when $c > c_h$). However, the density is unknown since it depends on the position of X which itself depends on c. Explicit solutions are unable to be written down succinctly. However an indication of the hypoxic region is illustrated in Fig. B.10(a).

B.2 Case $W < 1$

When the oxygen consumption rate is large enough, then $W < 1$ and a hypoxic region exists right from the start, with $X(0) = \sqrt{W}$. Then there exists a moving boundary $X(t)$ and a region $X(t) < x < 1$ which is hypoxic for some period of time such that $t > 0$. If $W/(4\lambda^2) > 1$, then initially $X(t)$ moves inward ($dX/dt < 0$) and the solutions are again given by (B.6–B.8). As before, eventually $X(t)$ will stop moving towards the left and the hypoxic region will retreat to the right. Alternatively, $W/(4\lambda^2) < 1$, making the oxygen consumption rate sufficiently large so that $X(t)$ can move outwards from the start ($dX/dt(0) > 0$) and the cell density remains at the initial (dimensionless) value of unity in the hypoxic region. These two cases are illustrated in Figs B.10(b–c). The example considered in Section 4.1 is the same type as in Fig. B.10(c).

Appendix C Travelling wave boundary layer analysis

A similar type of analysis to that performed by Pettet et al. (1996a) is undertaken here. This provides some insight into the nature of the travelling wave profiles illustrated in Fig. 8. The parameter values used in Fig. 8 are rescaled by a small parameter ϵ where $0 < \epsilon \ll 1$ as

$$(\mu_b, \mu_n) = \epsilon^3(\bar{\mu}_b, \bar{\mu}_n), \qquad \chi = \epsilon\bar{\chi}, \qquad (\kappa_1, \kappa_2) = \frac{1}{\epsilon^3}(\bar{\kappa}_1, \bar{\kappa}_2), \qquad \kappa_3 = \bar{\kappa}_3, \tag{C.1}$$

where $\epsilon = 0.1$ is appropriate for our example.

Introducing a travelling wave co-ordinate $z = x - \epsilon st$, the partial differential equations (32–34) can be transformed to ordinary differential equations, where ϵs is the wave speed. The new dependent variables are denoted as

$$N(z) = n(x,t), \qquad A(z) = a(x,t), \qquad B(z) = b(x,t). \tag{C.2}$$

After a change of variables, rescaling parameters and dropping overbars, the dominant terms in the model equations (32–34) become

$$-\epsilon s N_z = \left(\epsilon^3 \mu_n N_z - \epsilon \chi N A_z\right)_z + \epsilon^{-3}\kappa_1 AB - \epsilon^{-3}\kappa_2 N^2, \tag{C.3}$$

$$-\epsilon s A_z = -\kappa_3 AB, \tag{C.4}$$

$$-\epsilon s B_z = \epsilon^3 \mu_b (N B_z)_z - \epsilon^3 \mu_n N_z + \epsilon \chi N A_z, \tag{C.5}$$

subject to the conditions that N_z, A_z, and B_z are zero as $z \to \pm\infty$. We are interested in the region where the gradients of N, A, and B change rapidly; this defines the vascularisation front. We introduce a boundary layer variable ξ as

$$\xi = z/\epsilon. \tag{C.6}$$

Then in terms of the ξ variable (C.3–C.5) become:

$$-\epsilon^3 s N_\xi = \left(\epsilon^4 \mu_n N_\xi - \epsilon^2 \chi N A_\xi\right)_\xi + \kappa_1 AB - \kappa_2 N^2, \tag{C.7}$$

$$-s A_\xi = -\kappa_3 AB, \tag{C.8}$$

$$-s B_\xi = \epsilon \mu_b (N B_\xi)_\xi - \epsilon^2 \mu_n N_\xi + \chi N A_\xi. \tag{C.9}$$

As $\xi \to -\infty$, the system approaches the two steady states as

$$\text{vascularised state} \quad \xi \to -\infty, \quad (N, A, B) \to (0, 0, b_{-\infty}), \tag{C.10}$$

$$\text{avascular state} \quad \xi \to \infty, \quad (N, A, B) \to (0, 1, 0), \tag{C.11}$$

where $b_{-\infty}$ represents the blood vessel density in vascularised region of the scaffold.

The asymptotic behaviour of the solution for small ϵ is obtained from the leading order terms in (C.7–C.9) as

$$0 = \kappa_1 AB - \kappa_2 N^2, \tag{C.12}$$

$$s A_\xi = \kappa_3 AB, \tag{C.13}$$

$$-s B_\xi = \chi N A_\xi. \tag{C.14}$$

Clearly N can be written in terms of A and B as

$$N = \sqrt{\frac{\kappa_1}{\kappa_2} AB}. \tag{C.15}$$

Introducing a new parameter Ψ defined in (39), the equations (C.13) and (C.14) give

$$B = \Psi^2 \left(1 - A^{\frac{3}{2}}\right)^2, \tag{C.16}$$

$$A_\xi = \frac{\kappa_3}{s} A \left\{\Psi \left(1 - A^{\frac{3}{2}}\right)\right\}^2. \tag{C.17}$$

A relationship between vascularised density of blood vessels $b_{-\infty}$ and wave speed s is obtained from (C.16), namely

$$b_{-\infty} = \Psi^2. \tag{C.18}$$

Hence the vascularised density of blood vessels $b_{-\infty}$ is linked to a combination of the parameters in Ψ. An alternative expression gives the travelling wave speed as a function of $b_{-\infty}$ as

$$s = \frac{\chi}{3\sqrt{b_{-\infty}}}\sqrt{\frac{\kappa_1}{\kappa_2}}. \tag{C.19}$$

This equation remains unchanged when it is rescaled back to non-overbar variables in (C.1).

References

Agrawal, C.M., Ray, R.B., 2001. Biodegradable polymeric scaffolds for musculoskeletal tissue engineering. J. Biomed. Mater. Res. 55, 141–150.

Balding, D., McElwain, D.L.S., 1985. A mathematical model of tumour-induced capillary growth. J. Theor. Biol. 114, 53–73.

Boutilier, R.G., St-Pierre, J., 2000. Surviving hypoxia without really dying. Comp. Biochem. Physiol. Molecular Integr. Physiol. 126, 481–490.

Cassell, O.C.S., Morrison, W.A., Messina, A., Penington, A.J., Thompson, E.W., Stevens, G.W., Perera, J.M., Kleinman, H.D., Hurley, J.V., Romeo, R., Knight, K.R., 2001. The influence of extracellular matrix on the generation of vascularized, engineered, transplantable tissue. Ann. New York Acad. Sci. 944, 429–442.

Croll, T.I., Gentz, S., Müller, K., Davison, M., O'Connor, A.J., Stevens, G.W., Cooper-White, J., 2005. Modelling oxygen diffusion and cell growth in a porous, vascularising scaffold for soft tissue engineering applications. Chem. Eng. Sci. 60, 4924–4934.

Edelstein, L., 1982. The propagation of fungal colonies: a model for tissue growth. J. Theor. Biol. 98, 679–701.

Galban, C.J., Locke, B.R., 1997. Analysis of cell growth in a polymer scaffold using a moving boundary approach. Biotechnol. Bioeng. 56, 422–432.

Galban, C.J., Locke, B.R., 1999a. Analysis of cell growth kinetics and substrate diffusion in a polymer scaffold. Biotechnol. Bioeng. 65, 121–132.

Galban, C.J., Locke, B.R., 1999b. Effects of spatial variation of cells and nutrient and product concentrations coupled with product inhibition on cell growth in a polymer scaffold. Biotechnol. Bioeng. 64, 633–643.

Hasirci, V., Berthiaume, F., Bondre, S.P., Gresser, J.D., Trantolo, D.J., Toner, M., Wise, D.L., 2001. Expression of liver-specic functions by rat hepatocytes seededin treatedpoly (lactic-co-glycolic) acid biodegradable foams. Tissue Eng. 7, 385–394.

Kellner, K., Liebsch, G., Klimant, I., Wolfbeis, O.S., Blunk, T., Schulz, M.B., Göpferich, A., 2002. Determination of oxygen gradients in engineered tissue using a fluorescent sensor. Biotechnol. Bioeng. 80, 73–83.

Langer, R., Vacanti, J.P., 1993. Tissue engineering. Science 260, 920–926.

Lewis, M.C., MacArthur, B.D., Malda, J., Pettet, G., Please, C.P., 2005. Heterogeneous proliferation within engineered cartilaginous tissue: the role of oxygen tension. Biotechnol. Bioeng. 91, 607–615.

Malda, J., Woodfield, T.B.F., van der Vloodt, F., Kooy, F.K., Martens, D.E., Tramper, J., van der Blitterswijk, C.A., Riesle, J., 2004. The effect of PEGT/PBT scaffold architecture on oxygen gradients in tissue engineered cartilaginous constructs. Biomaterials 25, 5773–5780.

Murray, J.D., 2002. Mathematical Biology, vol. 1, 3rd edn. Springer, New York.

Patrick, C.W., 2000. Adipose tissue engineering: the future of breast and soft tissue reconstruction following tumor resection. Sem. Surg. Oncol. 19, 302–311.

Patrick, C.W., 2001. Tissue engineering strategies for adipose tissue repair. Anat. Rec. 263, 361–366.
Pettet, G.J., Byrne, H.M., McElwain, D.L.S., Norbury, J., 1996a. A model of wound-healing angiogenesis in soft tissue. Math. Biosci. 136, 35–63.
Pettet, G.J., Chaplain, M.A.J., McElwain, D.L.S., Byrne, H.M., 1996b. On the role of angiogenesis in wound-healing. Proc. Roy. Soc. Lond. B 263, 1487–1493.